The Journal of Chemical Physics

Two-color two-dimensional terahertz spectroscopy: A new approach for exploring even-order nonlinearities in the nonperturbative regime

Cite as: J. Chem. Phys. **154**, 154203 (2021); https://doi.org/10.1063/5.0047700
Submitted: 16 February 2021 • Accepted: 04 April 2021 • Published Online: 20 April 2021

Michael Woerner, Ahmed Ghalgaoui, Klaus Reimann, et al.

The Journal of Chemical Physics ARTICLE scitation.org/journal/jcp

Two-color two-dimensional terahertz spectroscopy: A new approach for exploring even-order nonlinearities in the nonperturbative regime

Cite as: J. Chem. Phys. 154, 154203 (2021); doi: 10.1063/5.0047700
Submitted: 16 February 2021 • Accepted: 4 April 2021 •
Published Online: 20 April 2021

Michael Woerner,[a] Ahmed Ghalgaoui,[b] Klaus Reimann,[c] and Thomas Elsaesser[d]

AFFILIATIONS

Max-Born-Institut für Nichtlineare Optik und Kurzzeitspektroskopie, 12489 Berlin, Germany

Note: This paper is part of the JCP Special Topic on Coherent Multidimensional Spectroscopy.
[a]**Author to whom correspondence should be addressed:** woerner@mbi-berlin.de
[b]**Electronic mail:** ghalgaou@mbi-berlin.de
[c]**Electronic mail:** reimann@mbi-berlin.de
[d]**Electronic mail:** elsasser@mbi-berlin.de

ABSTRACT

Nonlinear two-dimensional terahertz (2D-THz) spectroscopy at frequencies of the emitted THz signal different from the driving frequencies allows for exploring the regime of (off-)resonant even-order nonlinearities in condensed matter. To demonstrate the potential of this method, we study two phenomena in the nonlinear THz response of bulk GaAs: (i) The nonlinear THz response to a pair of femtosecond near-infrared pulses unravels novel fourth- and sixth-order contributions involving interband shift currents, Raman-like excitations of transverse-optical phonon and intervalence-band coherences. (ii) Transient interband tunneling of electrons driven by ultrashort mid-infrared pulses can be effectively controlled by a low-frequency THz field with amplitudes below 50 kV/cm. The THz field controls the electron–hole separation modifying decoherence and the irreversibility of carrier generation.

I. INTRODUCTION

Nonlinear two-dimensional infrared (2D-IR) spectroscopy of molecular ensembles in liquids and solids is currently dominated by studies of the third-order or $\chi^{(3)}$ response on femto- to picosecond time scales. This approach is based on three—in most cases resonant—interactions with the electric field of a two- or three-pulse sequence, generating a nonlinear signal. In particular, vibrational excitations of molecules in the liquid phase were extensively studied using both pump–probe and three-pulse photon-echo measurements.[1–5] Third-order spectroscopy of solids has combined femtosecond interband excitation of carriers with THz probing of intraband electron dynamics.[6,7] Phase-resolved 2D-THz spectroscopy has first focused on electronic excitations of solids, which are characterized by transition dipole moments orders of magnitude larger than those of vibrational transitions. A prototypical case is intersubband excitations in semiconductor quantum wells, displaying transition dipoles on the order of $e \cdot 10$ nm (e: elementary charge).[8–10] In such cases, moderate THz electric fields with amplitudes on the order of 1–50 kV/cm allow for driving light–matter interactions into the nonperturbative regime, well beyond the $\chi^{(3)}$ limit.

The nonperturbative regime of light–matter interactions is characterized by a stronger coupling of elementary excitations to the external THz field than the couplings between excitations of the system under study. Characteristic phenomena are Rabi oscillations, multi-photon absorption,[11,12] field-induced Wannier–Stark localization, and electron generation by field-induced tunneling processes,

with the latter three typically under nonresonant conditions.[13–18] In this range of interaction strengths, each of the applied driving pulses can interact several times with the sample before the nonlinear THz signal field is emitted. Such a behavior has been observed in 2D-THz experiments with the bulk semiconductor InSb, in which a sequence of three nonresonant THz pulses centered at 20 THz both drives two-TO-phonon coherences and induces multiple two-photon interband absorption events.[11,12] An analysis of the Liouville pathways underlying different interaction sequences demonstrates that the nonlinear response is of at least 11th order in the THz electric field. The nonlinear signal is emitted at the TO phonon frequency, which is different from the frequency of the driving THz pulses.

The two-color 2D-THz approach is applicable in a spectral range well beyond THz frequencies. A Raman-type excitation with femtosecond pulses in the visible or near-infrared range can induce a THz coherence, requiring at least two interactions with the driving field. For a nonzero transition dipole, the THz coherence emits an electric field, which can be detected in amplitude and phase as a function of real time t, e.g., by electro-optic sampling.[19,20] Introducing a pair of phase-locked nonresonant driving pulses at high frequency, which are separated by a delay time τ, allows for generating genuine 2D-THz spectra as a function of excitation frequency ν_τ and detection frequency ν_t. Here, the frequency domain 2D-THz spectra are derived from the time-domain THz signals by a 2D Fourier transform along τ and t. There is a minimum of four interactions with the two driving pulses to generate this type of 2D-THz spectrum. A detailed comparison of different experimental concepts using two-pulse, three-pulse, or even n-pulse schemes for studying both odd- and even-order nonlinearities of condensed matter systems has been given in a recent article.[21]

First experiments based on a two-color 2D-THz approach addressed the nonlinear THz response of bulk GaAs upon interaction with femtosecond near-infrared (NIR) pulses resonant to the electronic bandgap at 1.42 eV.[22] The second-order response induced by a single near-infrared pulse results in a coherent THz emission consisting of three components originating from (i) a time-dependent interband shift current,[23–25] (ii) a coherent polarization on transitions between the heavy- and light-hole valence bands, and (iii) a coherent TO-phonon polarization. Extending this study to the interaction of bulk GaAs with a pair of near-infrared pulses gives insight into the fourth-order THz response, which includes a frequency upshift of the TO phonon resonance due to local-field effects in the semiconductor crystal.[26] In this article, we present an in-depth analysis of the nonlinear THz response of bulk GaAs to a pair of femtosecond near-infrared pulses. Novel fourth- and sixth-order contributions to the nonlinear THz response are identified, in particular a component due to field-driven interband tunneling.

II. EVEN-ORDER NONLINEAR THz RESPONSE OF GaAs

The experimental concept of the two-color 2D-THz experiments is explained in Fig. 1. A pair of collinearly propagating NIR pulses A and B (linearly polarized along the $[1\bar{1}0]$ direction) excites a (111)-oriented bulk GaAs sample of 250 nm thickness mounted on a glass substrate. The emitted THz radiation from the sample is polarized along the $[11\bar{2}]$ direction, as

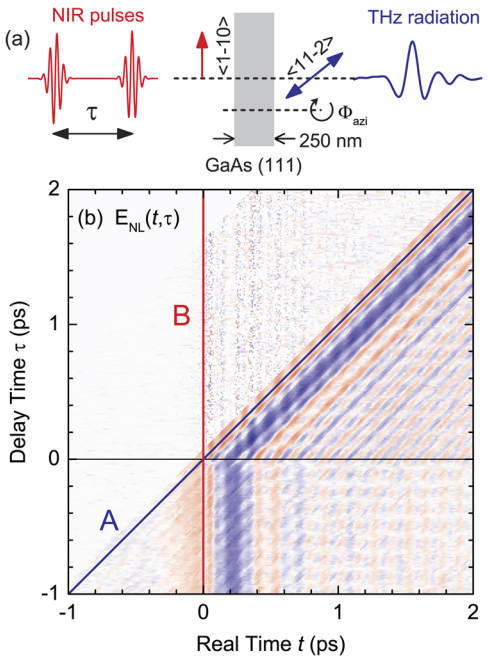

FIG. 1. (a) Concept of two-color 2D-THz experiments: two near-infrared pulses A and B separated by the coherence time τ are sent on a 250-nm-thick (111)-oriented GaAs layer. The subsequently emitted THz radiation polarized along the $[11\bar{2}]$ direction is measured by electro-optic sampling. (b) Contour plot of the emitted nonlinear THz signal $E_{NL}(t, \tau) = E_{THz,AB}(t, \tau) - E_{THz,A}(t, \tau) - E_{THz,B}(t)$ as a function of both the real time t and the delay time τ.

dictated by the space group $F\bar{4}3m$ of zinc blende.[22] The delay time τ between the two NIR pulses is measured relative to pulse B. For negative delay times ($\tau < 0$), pulse A interacts with the sample before pulse B. The THz field emitted by the sample is detected by phase-resolved electro-optic (EO) sampling with a weak NIR sampling pulse.[20,27] As in conventional 2D spectroscopy with two THz pulses, there are two independent time variables in this scheme, the delay time τ between the two excitation pulses and the real time t of the phase-resolved THz detection. The nonlinear THz emission signal is given by $E_{NL}(t, \tau) = E_{THz,AB}(t, \tau) - E_{THz,A}(t, \tau) - E_{THz,B}(t)$. Here, $E_{THz,AB}(t, \tau)$ is the electric field emitted after interaction with both near-infrared pulses, while $E_{THz,A}(t, \tau)$ and $E_{THz,B}(t)$ are the THz electric fields after interaction with only one of the two pulses. In the following, one needs to distinguish the electric-field amplitudes of the NIR driving pulses $E_{NIR,A}$ and $E_{NIR,B}$ from the electric-field transients of the nonlinear THz emission, $E_{THz,AB}(t, \tau)$, $E_{THz,A}(t, \tau)$, and $E_{THz,B}(t)$. A 2D Fourier transform of $E_{NL}(t, \tau)$ along τ and t generates 2D spectra of the THz emission as a function of the excitation frequency ν_τ and detection frequency ν_t.[8,28]

Femtosecond near-infrared pulses were generated at a 1 MHz repetition rate with an optical parametric amplifier (OPA; Opera-F, Light Conversion) pumped by an Yb-based laser system (Monaco, Coherent). We tuned the OPA output to a center frequency of ν_0 = 350 THz (850 nm) in the fundamental absorption edge of GaAs at room temperature. The NIR pulses were compressed to a duration of 25 fs and subsequently split into two excitation pulses

A and B and a third component, which serves as the probe pulse for EO sampling. For the experiments discussed in the following, we intentionally chose an asymmetric splitting ratio, i.e., pulse A and pulse B have pulse energies of 0.23 μJ and 0.18 μJ, respectively. Both beams have a Gaussian spatial profile with a diameter of 3 mm on the GaAs sample. From the fluences of pulses A and B and the optical thickness of the GaAs sample, one estimates a quasi-Fermi level of photoexcited electrons in the conduction band of around 40 meV, which corresponds to a maximum electron density below 10^{18} cm^{-3}. A 10 μm-thick (110)-oriented ZnTe crystal attached to a thick inactive (100)-oriented ZnTe substrate is used for EO sampling with a detection bandwidth of ~18 THz. All measurements are performed in a nitrogen atmosphere at ambient temperature (T = 300 K).

In Fig. 1(b), the nonlinear THz signal field $E_{NL}(t, \tau)$ is plotted as a function of delay time τ and real time t. The contour plot in Fig. 2 shows the 2D Fourier transform of $E_{NL}(t, \tau)$ as a function of the excitation frequency ν_τ (Fourier conjugate of delay time τ) and detection frequency ν_t (Fourier conjugate of real time t). This 2D-THz spectrum covers a frequency range of ν_τ = ±20 THz and ν_t = ±20 THz ("yellow" square in Fig. 2), which is limited along ν_τ by 500 time steps ($\Delta\tau$ = 10 fs) in scanning τ and along ν_t by the EO sampling detection bandwidth. In order to illustrate the origin of the observed nonlinear 2D signals, we have embedded the 2D-THz spectrum in a larger 2D plane covering also the frequency range of the near-infrared excitation pulses. To accommodate simultaneously both THz and laser frequencies in the very same 2D frequency plane, axis breaks at ν_τ = ±20 THz and ν_t = ±20 THz were introduced.

In a perturbative description of light–matter interactions, 2D spectra measured in a collinear beam geometry can be analyzed with the help of frequency vectors (ν_t, ν_τ) describing the driving electric fields $E_{NIR,A}(t, \tau)$ and $E_{NIR,B}(t)$ of pulses A and B at 350 THz and the different components of the emitted nonlinear THz signal $E_{NL}(t, \tau)$. The diagonal blue arrows in Fig. 2 stand for interaction events driven by pulse A, whereas the horizontal red arrows stand for those driven by pulse B. An odd-order nonlinear response, i.e., $\chi^{(2n+1)}$ with n = 1, 2, . . ., requires an odd number of interactions with either pulse A or pulse B, resulting in a detection frequency of the signal of $\nu_t \approx$ 350 THz (cf. orange $\chi^{(3)}$ spots in Fig. 2). As a result, the nonlinear signals occurring in the ν_τ = ±20 THz and ν_t = ±20 THz range must originate from even-order nonlinearities. The generation of the 2D-THz spectrum involves two interactions with each pulse A and pulse B, and thus, the 2D signals are, in the lowest order, $\chi^{(4)}$ contributions (red and blue). They are represented by frequency-vector chains involving at least four interactions. For a cross check, a 2D

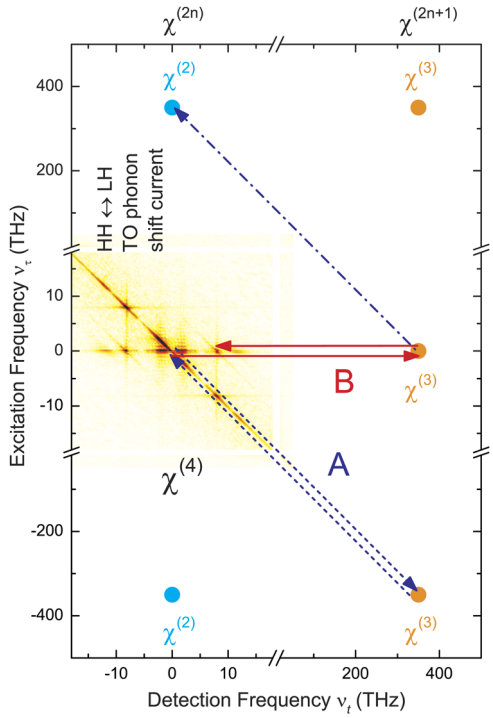

FIG. 2. Contour plot of the 2D Fourier transform of the measured nonlinear signal [Fig. 1(b)] as a function of the excitation frequency ν_τ and the detection frequency ν_t in a range of ±20 THz. The axis breaks have been introduced to accommodate both THz and near-infrared frequencies. The diagonal blue arrows stand for interaction events driven by 350 THz pulse A and the horizontal red arrows for those driven by 350 THz pulse B. Odd-order nonlinearities, e.g., $\chi^{(3)}$ (orange dots), end at $\nu_t \approx$ 350 THz (or higher). Analogously, the two-color 2D-THz experiment is not sensitive to a possible $\chi^{(2)}$ contribution (cyan dot) expected at $\nu_\tau \approx$ 350 THz. Experimentally observed $\chi^{(4)}$ contributions (red areas in the 2D spectrum) are represented by frequency-vector chains involving at least four interactions, i.e., two with pulse A (blue arrows) and two with pulse B (red arrows).

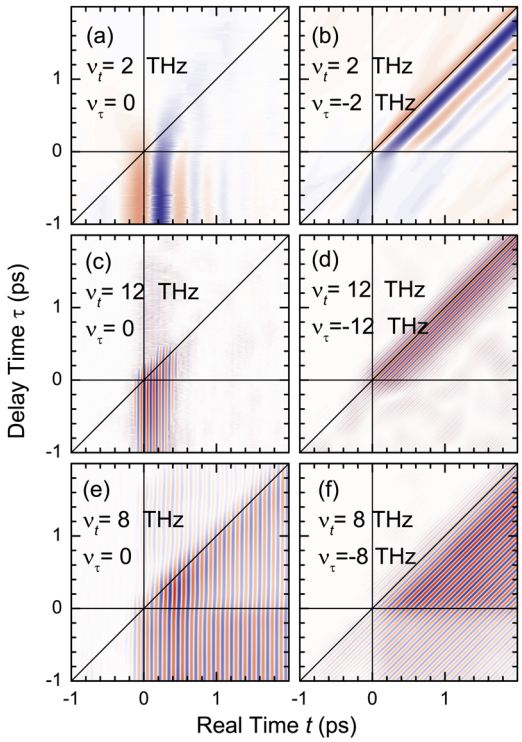

FIG. 3. Contour plot of $E_{NL}(t, \tau)$ on 2D-THz signal peaks at different frequency positions (ν_τ, ν_t). The transients represent the Fourier back-transforms of the frequency-filtered signal in the frequency domain (cf. Fig. 2).

experiment was performed with the sample rotated by $\Phi_{azi} = 60°$ [cf. Fig. 1(a)]. We observed the same 2D scan as in Fig. 1(b) but with a sign-inverted THz field, i.e., $E_{NL}^{60°}(t,\tau) = -E_{NL}^{0°}(t,\tau)$, as expected from the symmetry properties of even-order susceptibilities for the zinc-blende space group $F\bar{4}3m$ [cf. Eq. (2) and Fig. 2(b) of Ref. 22].

The 2D spectrum displays pronounced peaks at (ν_t, ν_τ) = (2, 0), (8, 0), (12, 0), (2, −2), (8, −8), and (12, −12) THz. This multitude of nonlinear signals is due to the simultaneous occurrence of different pathways by which the pair of 800-nm pulses interacts with the GaAs sample. A detailed discussion and analysis of the different contributions have been presented in Ref. 22. The signals at (2, 0) and (2, −2) THz represent the emission of an interband shift current, which is connected with the interband excitation of electron–hole pairs. The signals at (8, 0) and (8, −8) THz are due to coherent TO phonon excitations, which are excited via a Raman process within the spectral bandwidth of the 800-nm pulses and radiate via their THz transition dipole. The third group of rather weak signals at (12, 0) and (12, −12) THz originates from intervalence band HH-LH polarizations, again excited by a Raman process. Such interaction pathways are present in the nonlinear response to a single 800-nm pulse, i.e., the signal fields $E_{THz,A}(t,\tau)$ and $E_{THz,B}(t,\tau)$ as well. In the two-pulse experiment, however, the electron–hole plasma generated by the first 800-nm pulse modifies the interaction strength of the second 800-nm pulse, leading to a nonzero THz signal field $E_{NL}(t,\tau)$. Applying a Gaussian 2D-frequency filter on the individual signals and performing a 2D-Fourier back transform into the time domain, we derive the individual time-dependent signal fields shown in Figs. 3(a)–3(f).

As already mentioned, the energies and, thus, the electric fields of the two NIR pulses are different. As a consequence, the nonlinear THz response of GaAs depends on the pulse ordering, i.e., an A–B sequence induces a different response than a B–A sequence. In Fig. 4, electric field transients measured with an A–B pulse sequence (delay time τ = −1.4 ps) and a B–A pulse sequence (delay time τ = +1.4 ps) are compared. In addition, we show transients observed in single-pulse experiments with either pulse A or pulse B [panels (a), (d), and (g)], representing a second-order or $\chi^{(2)}$ response.

The $\chi^{(2)}$ signals due to the interband shift current [Fig. 4(a)] have a smaller amplitude for pulse B than for pulse A, reflecting the fact that the shift current is proportional to the intensity of the pulses. The 2D-THz signal in panel (b) (solid line) is generated by a B–A pulse sequence, in which pulse B excites an electron–hole plasma and the second pulse A excites a THz interband shift current.[22] The presence of the electron–hole plasma reduces the interband transition probability through Pauli blocking of the optically coupled states. As a result, the shift current amplitude generated by pulse A is reduced compared to an interaction

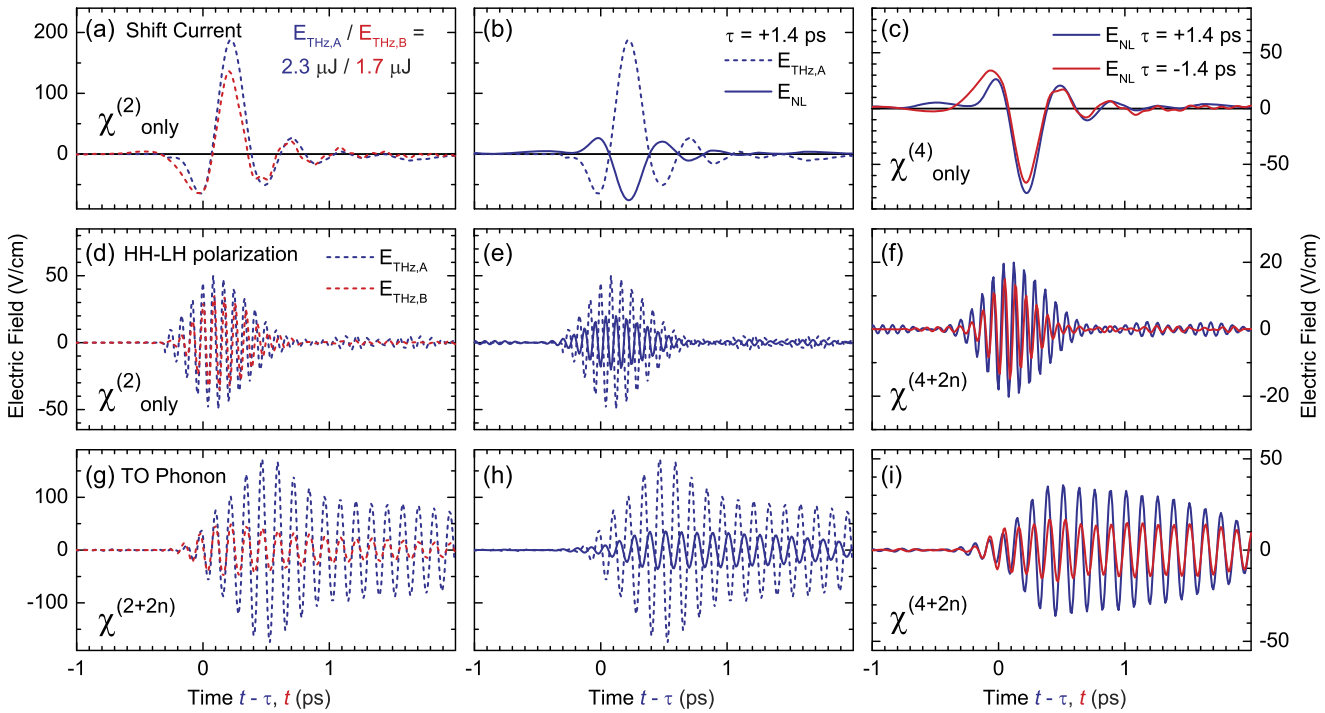

FIG. 4. Nonlinear THz signals emitted in response to a single NIR driving pulse (dashed lines) and nonlinear 2D-THz signals $E_{NL}(t,\tau)$ obtained in two-pulse experiments (solid lines). Blue curves: nonlinear THz signals $E_{THz,A}$ and E_{NL} observed for τ = +1.4 ps plotted as a function of the time difference $t - \tau$. Red curves: $E_{THz,B}$ and E_{NL} observed for τ = −1.4 ps plotted as a function of the real time t. (a)–(c) Shift current contribution to the emitted nonlinear THz signal. (d)–(f) Contribution of coherent HH ↔ LH intervalence band polarizations. (g)–(i) Contribution of coherent TO-phonon polarizations.

with an unpumped sample. This saturation of the shift current is reflected by the signal field $E_{NL}(t, \tau = +1.4$ ps) (solid line), which exhibits a phase opposite to the $\chi^{(2)}$ signal $E_{THz,A}$ (dashed line). Figure 4(c) compares the 2D-THz signals for A–B (red curve) and B–A (blue curve) pulse sequences. Because of their fourth-order ($\chi^{(4)}$) character, both signals are proportional to $E_{NL}^{SC} \propto E_{NIR,A}^2 E_{NIR,B}^2$, and thus, their amplitudes are identical within the experimental accuracy.

The THz transients due to coherent HH ↔ LH intervalence band polarizations are shown in Figs. 4(d)–4(f). The single-pulse ($\chi^{(2)}$) measurements [panel (d)] give a smaller amplitude for pulse B than for pulse A due to the smaller driving field of pulse B. Again, the signal generated by the B–A pulse sequence is smaller than the $\chi^{(2)}$ signal generated by pulse A [panel (e)]. Here, pulse B generates an electron–hole plasma and pulse A the HH ↔ LH polarization via a Raman process. This Raman process is resonantly enhanced by the interband transition dipole at the GaAs bandgap. Upon excitation of an electron–hole plasma by pulse B, the blueshift of the absorption edge leads to a reduction of resonance enhancement and a concomitant decrease in the signal amplitude compared to the $\chi^{(2)}$ case.

We now compare the HH ↔ LH nonlinear signals generated with the A–B and B–A pulse sequences [panel (f)]. In contrast to the identical shift current signals in the two cases [Fig. 4(c)], the A–B sequence induces a smaller nonlinear signal (red curve) than the B–A sequence (blue curve). This behavior is beyond a fourth-order ($\chi^{(4)}$) response and indicates that higher even-order

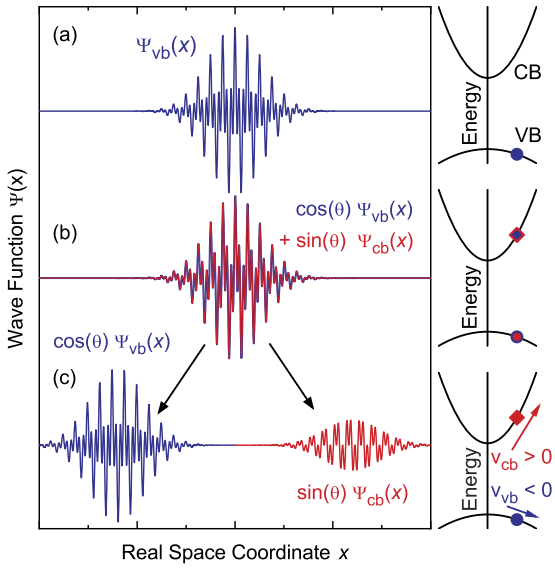

FIG. 5. Cartoon describing the tunneling process. (a) Wave function (schematically) of a valence band state at a certain wave vector (see the electronic band structure at the right). (b) An electric field leads to a coherent superposition of valence and conduction band states. (c) Since valence and conduction band states have velocities in real space in opposite directions (see arrows at the right), the valence and conduction band components of the coherent superposition state move apart from each other, leading to decoherence,[29–31] i.e., to an incoherent ensemble of electrons and holes.

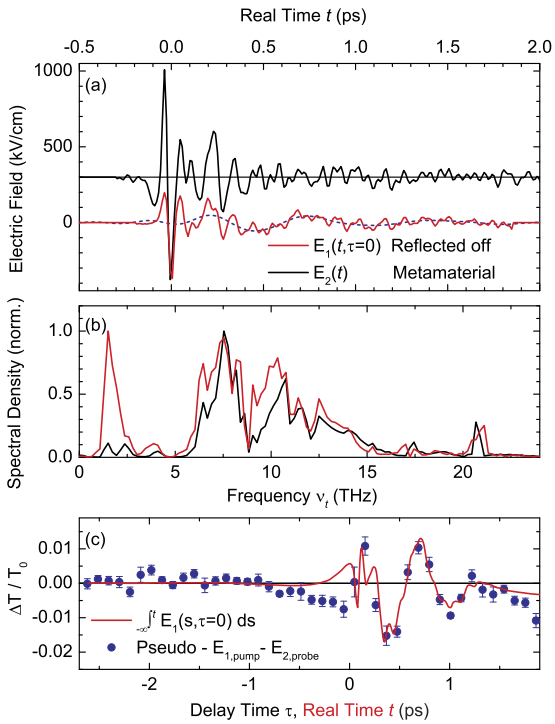

FIG. 6. (a) Electric-field transients of pulse 1 (red) and pulse 2 (black) after reflection from the sample. The dashed line shows the low-pass filtered pulse 1. (b) Corresponding pulse spectra (normalized). (c) Spectrally integrated pseudo-pump–probe signal $\Delta T/T_0$ (symbols) as a function of the delay time between both pulses. Red solid line: time integral of the electric field of pulse 1 at $\tau = 0$ as a function of real time t.

nonlinearities $\chi^{(4+2n)}$ must be present, a clear hallmark of the nonperturbative character of the underlying light–matter interaction. In addition to the saturation of the two-pulse nonlinear HH ↔ LH amplitude, one observes small differences in the

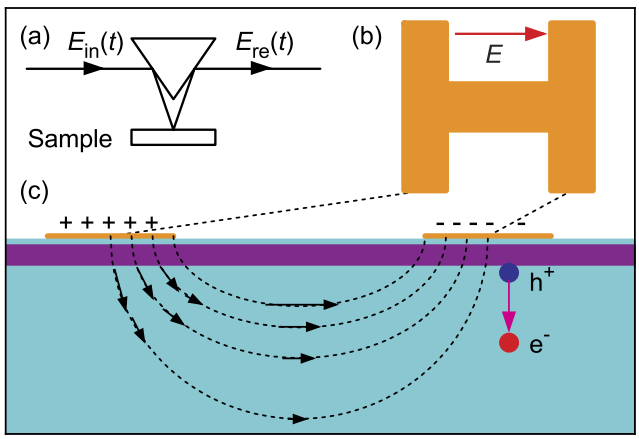

FIG. 7. (a) Schematic of the experimental setup. (b) Shape of the gold resonator structures that cover the top of the sample in a square array. (c) Arrows: electric fields inside the sample below the gold resonators. The sample has a 40 nm AlAs layer (violet) on top of a 300-μm thick GaAs layer (cyan).

temporal evolution of the phase of HH ↔ LH coherences in Figs. 4(e) and 4(f). Such phase changes point to excitation-induced frequency shifts of HH ↔ LH coherences, creating different nonlinear two-pulse THz signals. In a perturbative approach, a small deviation from a fourth-order two-pulse signal can be accommodated by adding a sixth-order ($\chi^{(6)}$) nonlinearity according to $E_{\mathrm{NL}}^{\mathrm{HH}\leftrightarrow\mathrm{LH}} \propto \chi^{(4)} E_{\mathrm{NIR,A}}^2 E_{\mathrm{NIR,B}}^2 + \chi^{(6)}\left(E_{\mathrm{NIR,A}}^4 E_{\mathrm{NIR,B}}^2 + E_{\mathrm{NIR,A}}^2 E_{\mathrm{NIR,B}}^4\right)$. The excitation-induced frequency shifts are a manifestation of many-body Coulomb correlations in the excited semiconductor. Another consequence of such correlations is interferences between the shift current and intervalence band nonlinearities.[22]

The nonlinear THz signals originating from the TO-phonon coherence [Figs. 4(g)–4(i)] are generated by a Raman process resonantly enhanced by the interband dipole moment. The single-pulse measurements [panel (g)] reveal a strong dependence of the $\chi^{(2)}$ signal on the driving field with a four times larger amplitude for pulse A compared to the weaker pulse B. The two-pulse data in Fig. 4(h) show a reduced amplitude and a significantly different phase evolution compared to the transient generated with the single pulse A. The phase differences are due to a frequency upshift of the TO-phonon resonance by the presence of an electron–hole-plasma, as has been discussed in detail in Ref. 26. The mechanism behind the frequency change is a local-field effect changing the dielectric function of the excited GaAs sample.

In summary, the results presented in this section demonstrate the potential of two-color 2D-THz spectroscopy for mapping the interplay and coupling of pathways of nonlinear light–matter interactions by dissecting nonlinearities up to high orders in the optical field. In the case studied here, many-body Coulomb correlations and the resulting local field effects are the predominant mechanisms leading to such a complex behavior.

III. TRANSIENT INTERBAND TUNNELING OF ELECTRONS DRIVEN BY TWO-COLOR TERAHERTZ FIELDS

Strong THz pulses with an electric field amplitude on the order of 300 kV/cm induce interband tunneling of electrons from the valence band into the conduction band of GaAs.[14] The irreversibility of THz-field-induced tunneling, a necessary requirement for a persistent carrier population, is to a large extent determined by spatio-temporal aspects concerning the charge separation of the electron from the remaining hole. As shown in Ref. 14, THz-field-induced electron–hole generation involves two mechanisms as follows (Fig. 5):

(i) The strong THz field generates a coherent superposition of valence- and conduction-band states [Fig. 5(b)], a mechanism that corresponds to the creation of "virtual" electron–hole pairs. If this electric field is reversed within a short period of time, the recombination of the "virtual" electron–hole pairs is fully reversible, i.e., no real carriers are generated.

(ii) The THz field spatially separates the electron and hole [Fig. 5(c)]. This transfers them into different environments, leading to different fluctuations experienced by the two parts. This has the result that the recombination of the THz-generated "virtual" electron–hole pair is no longer fully reversible, i.e., decoherence has occurred and a real electron–hole pair arises. Seminal theoretical work[29–31] has shown that the decoherence rate grows quadratically with the spatial

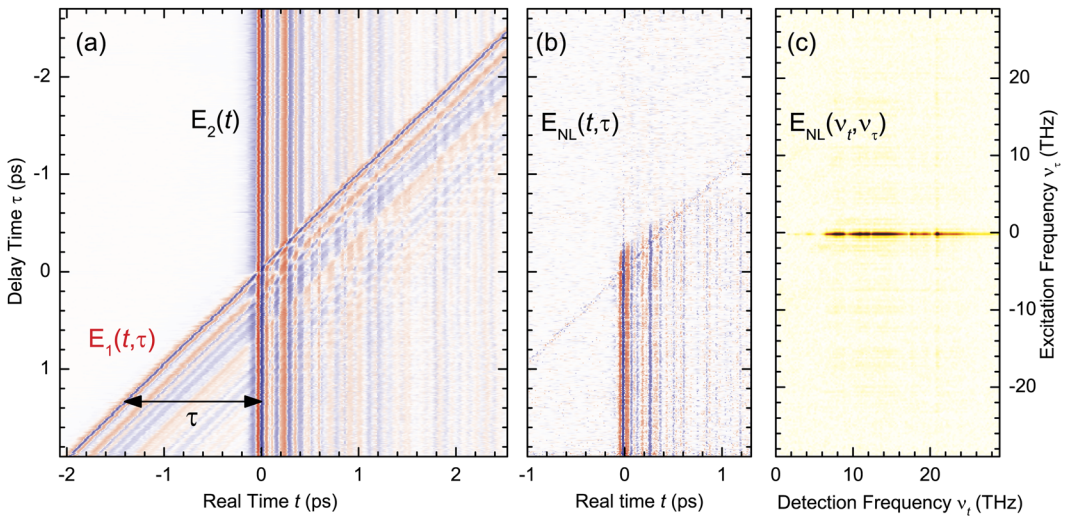

FIG. 8. Two-color 2D-THz spectroscopy on GaAs exposed to electric THz/MIR and MIR fields enhanced by an appropriate gold metamaterial using the two pulses shown in Fig. 6. (a) Contour plot of the sum of electric field transients $E_1(t, \tau) + E_2(t)$ reflected off the sample as a function of the delay time τ and the real time t. (b) Nonlinear signal $E_{\mathrm{NL}}(t, \tau)$. The linear amplitude scales of the 2D plots range over (a) ±900 and (b) ±15 kV/cm. (c) Contour plot of the amplitude $|E_{\mathrm{NL}}(\nu_t, \nu_\tau)|$ obtained from a 2D Fourier transform of $E_{\mathrm{NL}}(t, \tau)$.

separation between the electron and hole. Since the separation caused by an electric field oscillating with the frequency ν is proportional to $1/\nu^2$, THz fields with their low frequencies are powerful tools to enhance the irreversibility of electron–hole generation.

A first experimental probe of electron–hole pairs generated by field-induced tunneling is the THz-induced luminescence of the GaAs sample.[16] As an alternative, one can use the nonlinear THz absorption due to the electron–hole plasma because the absorbed energy is a measure of the THz-induced electron–hole density.[14] In the following, we discuss two-color 2D-THz experiments performed with a two-pulse sequence. The results give new insight into the interplay of THz-driven interband and intraband motions of carriers and demonstrate that the irreversibility of carrier generation by the mid-infrared pulse can be effectively controlled by the low-frequency components of the THz pulse.

The time-resolved electric fields $E_1(t, \tau)$ and $E_2(t)$ of pulses 1 and 2 are presented in Fig. 6(a), and their normalized spectra are shown in Fig. 6(b). Both spectra have a strong mid-infrared component between 5 and 22 THz, corresponding to the spike-like structure of the time-dependent electric fields at the onset of the pulses around $t = 0$. The maximum electric-field amplitude of pulse 2 is two times higher than that of pulse 1. As a result, when applying pulse 2 alone to the sample, it generates an appreciable carrier density by field-induced interband tunneling,[16] i.e., a pronounced nonlinear single-pulse response. In contrast, pulse 1 creates an order of magnitude lower electron–hole density. On the other hand, pulse 1 possesses a pronounced component around 2 THz, which is absent in pulse 1. The two pulses travel collinearly and interact in p-polarization with the sample in a reflection geometry at an angle of incidence of 20° [Fig. 7(a)]. The pulses reflected from the sample are detected by EO sampling in ZnTe. For positive delay times τ, pulse 1 interacts with the sample before pulse 2.

The sample studied here (Fig. 7) is similar to that used in Ref. 33. It consists of a gold metastructure on top, a 40-nm thick AlAs layer, and a 300-μm thick GaAs layer. The AlAs layer suppresses electron tunneling from the gold metamaterial into the semiconductor, allowing for the observation of THz-induced tunneling in the "surface-free" thick GaAs layer. The sample surface is covered with an array of gold resonator structures [Fig. 7(b)], forming a metasurface. In the present experiment, the metasurface is used to enhance the electric-field strength in the thick GaAs layer. The field enhancement is frequency dependent and has its highest values at the edges and corners of the metal resonators. A field enhancement around 12 THz by a factor of 15 and around 2 THz by a factor of 5 is estimated from finite element calculations for a similar sample structure.[33] The field amplitude decays "exponentially" into the semiconductor structure on a length scale of typically ≈100 nm.

The results of the two-color 2D experiments are presented in Fig. 8. In the 2D scans, we apply both pulses to the sample and measure the nonlinearly emitted electric field $E_{\mathrm{NL}}(t, \tau) = E_{\mathrm{both}}(t, \tau) - E_1(t, \tau) - E_2(t)$ [Fig. 8(b)] as a function of real time t and delay time τ [Fig. 8(a)]. $E_{\mathrm{both}}(t, \tau)$ is the electric field reflected from the sample when both pulses are incident on the sample, $E_1(t, \tau)$ the field when only pulse 1 is present and $E_2(t)$ the field when only pulse 2 is present. Figure 8(c) shows the amplitude of the 2D Fourier transform $|\hat{E}_{\mathrm{NL}}(\nu_t, \nu_\tau)|$ of the nonlinear signal of Fig. 8(b). The nonlinear signal has significant contributions only for $|\nu_\tau| < 2$ THz and for 5 THz $< |\nu_t| <$ 25 THz.

Along the lines of conventional pump–probe spectroscopy (with weak probe pulses), we define a spectrally resolved pseudo-pump–probe signal in the nonperturbative regime according to

$$\frac{\Delta T(\nu_t, \tau)}{T_0(\nu_t)} = 2\,\mathrm{Re}\left[\frac{E_{\mathrm{NL}}(\nu_t, \tau)E_2^*(\nu_t)}{E_2(\nu_t)E_2^*(\nu_t)}\right]. \quad (1)$$

Note that $E_2(\nu_t)$ in Eq. (1) is a nonlinear signal field containing contributions from the incident pulse 2 and the linear and nonlinear sample responses, a fact that distinguishes the pseudo-pump–probe signal from the conventional pump–probe signal.

Figure 9 shows a contour plot [panel (a)] and cuts [panel (b)] for two fixed delay times τ of the spectrally resolved pseudo-pump–probe signal. As a function of the delay time τ, pulse 2 experiences a modulation of its nonlinear, broadband absorption, which originates from interband tunneling of carriers.[32] In Fig. 6(c), we plot

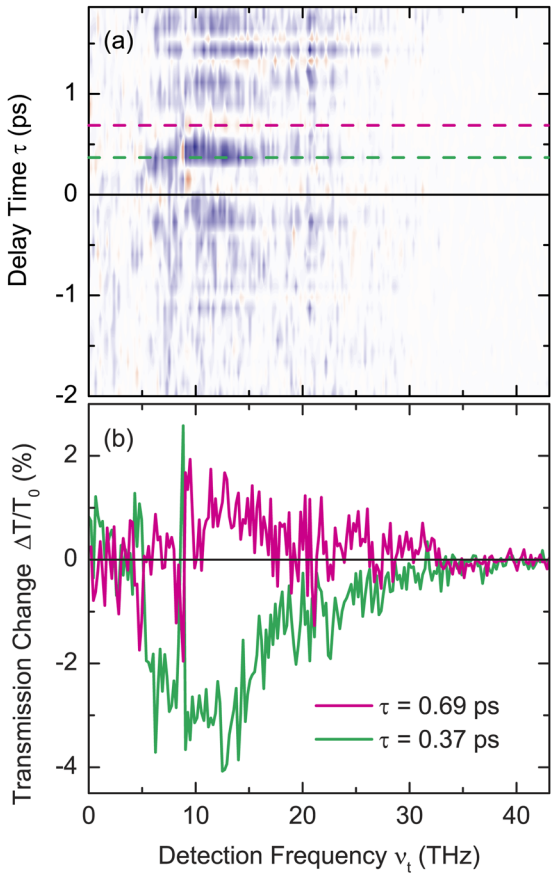

FIG. 9. (a) Contour plot of the spectrally resolved pseudo-pump–probe signal according to Eq. (1). (b) Horizontal cuts for the two delay times τ marked by dashed lines in (a), showing either induced absorption (for $\tau = 0.37$ ps) or bleaching (for $\tau = 0.69$ ps).[32]

the spectrally integrated pseudo-pump-probe signal (symbols with error bars) together with the time integral of the electric field, i.e., the vector potential of pulse 1, $A_1(t, \tau = 0) = \int_{-\infty}^{t} E_1(s, \tau = 0)ds$. For positive delay times τ, the vector-potential transient $A_1(t, \tau = 0) = A_1(t = 0, \tau)$ (due to the symmetry of the 2D scan) agrees almost perfectly with the spectrally integrated transmission change of pulse 2. This shows that the nonlinear pseudo-pump-probe signal is linear in the electric-field amplitude of pulse 1, another peculiarity of the pseudo-pump-probe signal. Since the nonlinear signal occurs in the same frequency range as the spectrum of pulse 2, the interaction with pulse 2 has to be of odd order. Otherwise, the nonlinear signal would have frequency components at twice the frequency of pulse 2. Overall, the experimentally observed pseudo-pump–probe signal in Fig. 6(c) corresponds to even-order nonlinear response functions.

For electric fields along the [100] direction of a bulk GaAs crystal, all even-order nonlinearities yield zero nonlinear polarizations. In our sample, even-order nonlinearities become possible for two reasons: (i) the metastructure introduces longitudinal components of the electric fields [Fig. 7(c)], which allow for nonlinear polarizations, and (ii) the electron–hole pair generation occurs very near the GaAs/AlAs interface. This interface reduces the symmetry, allowing for nonlinear polarizations of even order.

The interpretation of the two-color 2D-THz experiment is straightforward. Interband tunneling of carriers is induced by the strong field of pulse 2. The electric-field amplitude of the short spike at the onset of pulse 2 determines the density of "virtual" electron–hole pairs. To transform them in real electron–hole pairs, decoherence by spatial separation in the electric field (or vector potential) of pulse 1 is required. The vector potential of pulse 1 has a large amplitude, which allows for a large spatial separation by 100 nm and more of the electron from the hole. As a result, the phase of the vector potential $A_1(t, \tau = 0)$ controls the irreversibility of the field-induced interband tunneling induced by pulse 2, the carrier density, and the related absorption of pulse 2. Interestingly, interband tunneling induced by pulse 2 can be enhanced, resulting in induced absorption at $\tau = 0.37$ ps [green curve in Fig. 9(a)], or be reduced (at $\tau = 0.69$ ps, magenta curve). In other words, the sub-2.5 THz component of pulse 1 allows for steering the rate of interband tunneling and thus the eventual carrier density.

IV. CONCLUSIONS AND OUTLOOK

In conclusion, two-color 2D-THz spectroscopy expands the application range of nonlinear THz spectroscopy substantially and, in particular, allows for studying even-order nonlinearities of the fourth and/or higher order. The prototypical applications discussed here show that even moderate field amplitudes of THz pulses can induce a highly nonlinear response, benefitting from the comparably long interaction periods with the sample and, in the case of phonon excitations, picosecond decoherence times. While we have focused here on elementary excitations in a bulk semiconductor, the two-color 2D-THz approach is applicable for molecular systems as well, e.g., by combining Raman-type excitations of vibrations with the phase-resolved detection of THz or mid-infrared emission.

So far, the potential of two-color 2D-THz spectroscopy for studying even-order nonlinearities has not been exploited fully. In the 2D spectrum shown in Fig. 2, the second-order (i.e., $\chi^{(2)}$) signal located around the $(\nu_t, \nu_\tau) = (0, 350)$ THz 2D-frequency vector has not been explored in detail. At this frequency position, interference phenomena between ultrafast shift currents, the TO-phonon, and HH ↔ LH intervalence band polarizations contribute to the signal and give insight into Coulomb correlations in the excited semiconductor. Using a pair of truly phase-locked near-infrared pulses and performing 2D scans with time steps in t and τ on the order of 0.1 fs would allow for deciphering interferences of the nonlinear components in fine detail. Another possible extension of the present concept is nonlinear 2D (or even 3D) experiments with three driving pulses. Concerning even-order nonlinearities, one might think about three-pulse Raman-echo experiments for studying the TO-phonon resonance. Such a scheme would correspond to a sixth-order (i.e., $\chi^{(6)}$) nonlinear response of the crystal.

ACKNOWLEDGMENTS

We thank our colleagues who were involved in earlier parts of this research, in particular, Klaus Biermann, Igal Brener, Giulia Folpini, Christos Flytzanis, Peter Liu, and Carmine Somma. We acknowledge funding from the Deutsche Forschungsgemeinschaft (Grant No. WO 558/14-1).

DATA AVAILABILITY

The data that support the findings of this study are available from the corresponding author upon reasonable request.

REFERENCES

[1] S. Mukamel, "Multidimensional femtosecond correlation spectroscopies of electronic and vibrational excitations," Annu. Rev. Phys. Chem. **51**, 691–729 (2000).
[2] D. M. Jonas, "Two-dimensional femtosecond spectroscopy," Annu. Rev. Phys. Chem. **54**, 425–463 (2003).
[3] P. Hamm and M. Zanni, *Concepts and Methods of 2D Infrared Spectroscopy* (Cambridge University Press, Cambridge, 2011).
[4] M. Cho, *Two-Dimensional Optical Spectroscopy* (CRC Press, Boca Raton, 2009).
[5] *Coherent Multidimensional Spectroscopy*, edited by M. Cho (Springer, Singapore, 2019).
[6] M. C. Beard, G. M. Turner, and C. A. Schmuttenmaer, "Transient photoconductivity in GaAs as measured by time-resolved terahertz spectroscopy," Phys. Rev. B **62**, 15764–15777 (2000).
[7] R. Huber, F. Tauser, A. Brodschelm, M. Bichler, G. Abstreiter, and A. Leitenstorfer, "How many-particle interactions develop after ultrafast excitation of an electron-hole plasma," Nature **414**, 286–289 (2001).
[8] W. Kuehn, K. Reimann, M. Woerner, and T. Elsaesser, "Phase-resolved two-dimensional spectroscopy based on collinear *n*-wave mixing in the ultrafast time domain," J. Chem. Phys. **130**, 164503 (2009).
[9] W. Kuehn, K. Reimann, M. Woerner, T. Elsaesser, R. Hey, and U. Schade, "Strong correlation of electronic and lattice excitations in GaAs/AlGaAs semiconductor quantum wells revealed by two-dimensional terahertz spectroscopy," Phys. Rev. Lett. **107**, 067401 (2011).
[10] G. Folpini, D. Morrill, C. Somma, K. Reimann, M. Woerner, T. Elsaesser, and K. Biermann, "Nonresonant coherent control—Intersubband excitations manipulated by a nonresonant terahertz pulse," Phys. Rev. B **92**, 085306 (2015).
[11] C. Somma, G. Folpini, K. Reimann, M. Woerner, and T. Elsaesser, "Two-phonon quantum coherences in indium antimonide studied by nonlinear two-dimensional terahertz spectroscopy," Phys. Rev. Lett. **116**, 177401 (2016).
[12] C. Somma, G. Folpini, K. Reimann, M. Woerner, and T. Elsaesser, "Phase-resolved two-dimensional terahertz spectroscopy including off-resonant interactions beyond the $\chi^{(3)}$ limit," J. Chem. Phys. **144**, 184202 (2016).

[13]W. Kuehn, P. Gaal, K. Reimann, M. Woerner, T. Elsaesser, and R. Hey, "Coherent ballistic motion of electrons in a periodic potential," Phys. Rev. Lett. **104**, 146602 (2010).
[14]W. Kuehn, P. Gaal, K. Reimann, M. Woerner, T. Elsaesser, and R. Hey, "THz-induced interband tunneling of electrons in GaAs," Phys. Rev. B **82**, 075204 (2010).
[15]F. Junginger, B. Mayer, C. Schmidt, O. Schubert, S. Mährlein, A. Leitenstorfer, R. Huber, and A. Pashkin, "Nonperturbative interband response of a bulk InSb semiconductor driven off resonantly by terahertz electromagnetic few-cycle pulses," Phys. Rev. Lett. **109**, 147403 (2012).
[16]C. Lange, T. Maag, M. Hohenleutner, S. Baierl, O. Schubert, E. R. J. Edwards, D. Bougeard, G. Woltersdorf, and R. Huber, "Extremely nonperturbative nonlinearities in GaAs driven by atomically strong terahertz fields in gold metamaterials," Phys. Rev. Lett. **113**, 227401 (2014).
[17]C. Schmidt, J. Bühler, A.-C. Heinrich, J. Allerbeck, R. Podzimski, D. Berghoff, T. Meier, W. Schmidt, C. Reichl, W. Wegscheider, D. Brida, and A. Leitenstorfer, "Signatures of transient Wannier-Stark localization in bulk gallium arsenide," Nat. Commun. **9**, 2890 (2018).
[18]A. Ghalgaoui, L.-M. Koll, B. Schütte, B. P. Fingerhut, K. Reimann, M. Woerner, and T. Elsaesser, "Field-induced tunneling ionization and terahertz-driven electron dynamics in liquid water," J. Phys. Chem. Lett. **11**, 7717–7722 (2020).
[19]Q. Wu and X.-C. Zhang, "Free-space electro-optic sampling of terahertz beams," Appl. Phys. Lett. **67**, 3523–3525 (1995).
[20]Q. Wu and X.-C. Zhang, "Free-space electro-optics sampling of mid-infrared pulses," Appl. Phys. Lett. **71**, 1285–1286 (1997).
[21]K. Reimann, M. Woerner, and T. Elsaesser, "Two-dimensional terahertz spectroscopy of condensed-phase molecular systems," J. Chem. Phys. **154**, 120901 (2021).
[22]A. Ghalgaoui, K. Reimann, M. Woerner, T. Elsaesser, C. Flytzanis, and K. Biermann, "Resonant second-order nonlinear terahertz response of gallium arsenide," Phys. Rev. Lett. **121**, 266602 (2018).
[23]A. M. Glass, D. von der Linde, and T. J. Negran, "High-voltage bulk photovoltaic effect and the photorefractive process in $LiNbO_3$," Appl. Phys. Lett. **25**, 233–235 (1974).
[24]R. von Baltz and W. Kraut, "Theory of the bulk photovoltaic effect in pure crystals," Phys. Rev. B **23**, 5590–5596 (1981).
[25]C. Somma, K. Reimann, C. Flytzanis, T. Elsaesser, and M. Woerner, "High-field terahertz bulk photovoltaic effect in lithium niobate," Phys. Rev. Lett. **112**, 146602 (2014).
[26]A. Ghalgaoui, K. Reimann, M. Woerner, T. Elsaesser, C. Flytzanis, and K. Biermann, "Frequency upshift of the transverse optical phonon resonance in GaAs by femtosecond electron-hole excitation," Phys. Rev. Lett. **125**, 027401 (2020).
[27]K. Reimann, R. P. Smith, A. M. Weiner, T. Elsaesser, and M. Woerner, "Direct field-resolved detection of terahertz transients with amplitudes of megavolts per centimeter," Opt. Lett. **28**, 471–473 (2003).
[28]T. Elsaesser, K. Reimann, and M. Woerner, *Concepts and Applications of Nonlinear Terahertz Spectroscopy* (Morgan & Claypool Publishers, San Rafael, CA, 2019).
[29]A. O. Caldeira and A. J. Leggett, "Path integral approach to quantum Brownian motion," Physica A **121**, 587–616 (1983).
[30]W. H. Zurek, "Decoherence and the transition from quantum to classical—Revisited," Los Alamos Sci. **27**, 86–109 (2002).
[31]W. H. Zurek, "Decoherence, einselection, and the quantum origins of the classical," Rev. Mod. Phys. **75**, 715–775 (2003).
[32]The spectral dip around 8 THz is due to the strong absorption of TO phonons in GaAs and not related to carrier dynamics.
[33]M. Woerner, C. Somma, K. Reimann, T. Elsaesser, P. Q. Liu, Y. Yang, J. L. Reno, and I. Brener, "Terahertz driven amplification of coherent optical phonons in GaAs coupled to a metasurface," Phys. Rev. Lett. **122**, 107402 (2019).